Effects of Battery Buffering on the Post-Load-Transient Performance of a PSOFC

Sudip K. Mazumder, *Senior Member, IEEE*, Sanjaya K. Pradhan, *Student Member, IEEE*, Joseph Hartvigsen, Michael R. von Spakovsky, and Diego F. Rancruel

***Abstract*—For a planar solid-oxide fuel cell (PSOFC)-based power system, the differences in the response times of the PSOFC stack, the power electronics subsystem (PES), and the balance-of-plant subsystem (BOPS) cause low-reactant conditions near the PSOFC electrodes during load transients. Because the BOPS cannot instantaneously provide enough fuel to the PSOFC, the load transients have a detrimental effect on the performance and life of the fuel cell. To alleviate the degrading effects of load transients on PSOFC stacks, the effectiveness of the energy buffering is investigated.**

***Index Terms*—Balance-of-plant subsystem (BOPS), distributed generation (DG), energy buffering, load transient, mitigation, planar solid-oxide fuel cell (PSOFC), power conditioning system (PCS), power electronics.**

NOMENCLATURE

AL	Application load.
ASR	Area-specific resistance ($\Omega \cdot \mathrm{cm}^2$).
BOPS	Balance-of-plant subsystem.
C_p	Specific heat capacity at constant pressure ($\mathrm{J \cdot kg^{-1} \cdot {}^\circ C^{-1}}$).
CTE	Coefficient of thermal expansion.
DG	Distributed generation.
En	Nernst potential (V).
F	Faraday's electrochemical constant (C).
FPS	Fuel-processing subsystem.
I	PSOFC output current (A).
ji	Current density in the 1-D cell model ($\mathrm{A \cdot cm^{-2}}$).
η	Hydrogen molar flow rate ($\mathrm{mol \cdot s^{-1}}$).
PCS	Power-conditioning system.
PES	Power-electronics subsystem.
PHT	Pressurized hydrogen tank.
PSOFC	Planar solid-oxide fuel cell.
PSOFCS	Planar solid-oxide fuel cell stack.
Q	Heat rate per unit volume ($\mathrm{W \cdot m^{-3}}$).
ρ	Mass density ($\mathrm{kg \cdot m^{-3}}$).
T_∞	Enclosure temperature (K).
$T_{n,t}$	Temperature at the nth segment at the instant t (K).
U	Hydrogen utilization, dimensionless.
V_{op}	Output voltage (V).
V_{tn}	Thermal neutral voltage (V).
Δx	Incremental step distance (m).
x, z	Spatial dimensions of the PSOFC used in the finite element model (mm).

Manuscript received October 20, 2004; revised January 11, 2006. This work was supported in part by the U.S. Department of Energy (DoE), under Award DE-FC2602NT41574 and in part by the National Science Foundation under CAREER Award 0239131 given to S. K. Mazumder in the year 2003. This paper was presented in part by at the IEEE Power Electronics Specialists Conference 2004. Any opinions, findings, conclusions, or recommendations expressed herein are those of the authors and do not necessarily reflect the views of the DoE. Paper no. TEC-00296-2004.

S. K. Mazumder and S. K. Pradhan are with the Laboratory for Energy and Switching Electronics Systems (LESES), Department of Electrical and Computer Engineering, University of Illinois, Chicago, IL 60607-7053 USA (e-mail: mazumder@ece.uic.edu; spradh1@uic.edu).

J. Hartvigsen is with Ceramatec Inc., Salt Lake City, UT 84119 USA (e-mail: jjh@ceramatec.com).

M. R. von Spakovsky is with the Department of Mechanical Engineering, Center for Energy Systems Research, Virginia Polytechnic Institute and State University, Blacksburg, VA 24061 USA (e-mail: vonspako@vt.edu).

D. F. Rancruel is with General Electric Power Generation, Greenville, SC 29602 USA (e-mail: Diego.RancruelArce@ge.com).

Digital Object Identifier 10.1109/TEC.2006.876420

I. INTRODUCTION

OVER the last few years, fuel cells and fuel-cell based PCSs have been the subject of extensive research for meeting the increasing demands of power quality and reliability for DG systems. This is because fuel cells have several advantages including high energy efficiency, near-zero emissions, ease of installation in urban as well as in remote regions, silent operation, and fewer moving parts [1], [2]. Although several fuel cells are being considered for DG, PSOFCs, as illustrated in Fig. 1 at cell and stack levels and explained in detail in [3], are emerging as one of the prime candidates, primarily because of their high energy efficiency and simple power generation architecture.

However, for commercial use, SOFC technology, as per the U.S. Department of Energy (DoE) guidelines, needs to demonstrate an operating life of greater than 40 000 h for stationary applications and greater than 5000 h for transportation applications. Recently, using a comprehensive model of the tubular SOFC PCS [4], Acharya *et al*. [5], [6], von Spakovsky *et al*. [7], and Mazumder *et al*. [8] have demonstrated that transients in the output current of the PES may have a significant impact on the life of the SOFC stack because of the following reasons.

1) BOPS cannot react instantaneously to the increased fuel demands during load transients, leading to low-reactant conditions [8], [9] within the SOFCS. This causes the reoxidation of the anode, which degrades the PSOFC [13].
2) With the fuel utilization of a stack changing drastically due to a load transient, a safer and lower operating fuel utilization is enforced to prevent zero-reactant condition in the PSOFCS. Because the efficiency of a stack depends on the operating stack fuel utilization [14], lower operating fuel utilization reduces the efficiency of the stack.

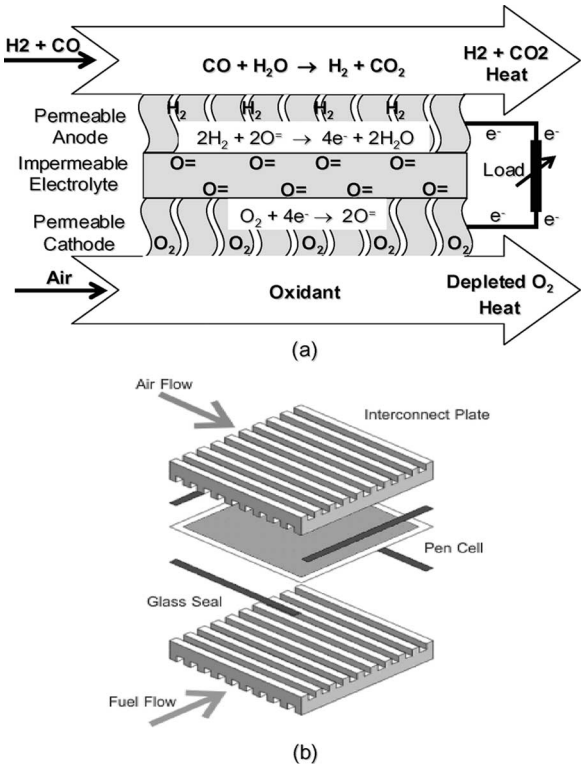

Fig. 1. (a) Principle of operation of the PSOFC. (b) Illustration of a repeat cell element in a PSOFCS.

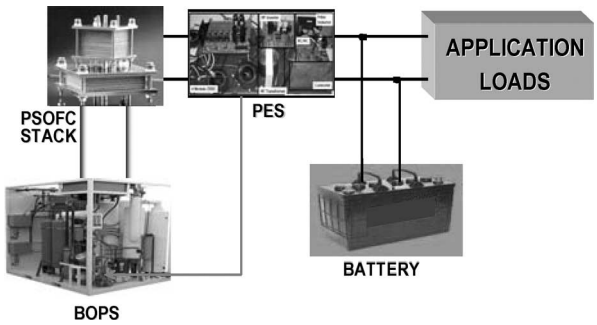

Fig. 2. Block diagram of a complete PSOFC PCS comprised of a PSOFCS PES and BOPS supplying power to the AL.

3) The abnormal rise in the PSOFC temperature due to higher current density in the stack induces residual stresses [11] that degrade its reliability.

Thus, there exists a need for mitigation techniques that can alleviate the impacts of these degrading effects on the reliability and performance of PSOFC stack during a load transient. Toward the end of the paper, a detailed thermochemical analysis of the impact of the load transient on a PSOFCS is provided. The effects of the load transient on the fuel utilization, current density, and temperature with and without the battery buffering are investigated. The battery provides the additional load current during the transient and alleviates the effect of the load transient on these parameters, thereby avoiding any degrading effects. The analyses in this paper may lead to the choice of battery size and optimal design and operation of the PSOFC PCS (as shown in Fig. 2).

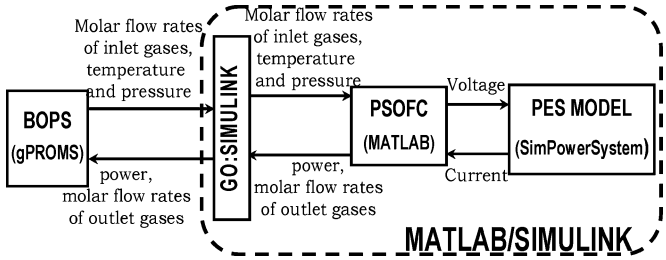

Fig. 3. Schematic showing the implementation of a comprehensive PSOFC-PCS model with the flow of data among simulation models using gPROMS and MATLAB/Simulink platforms.

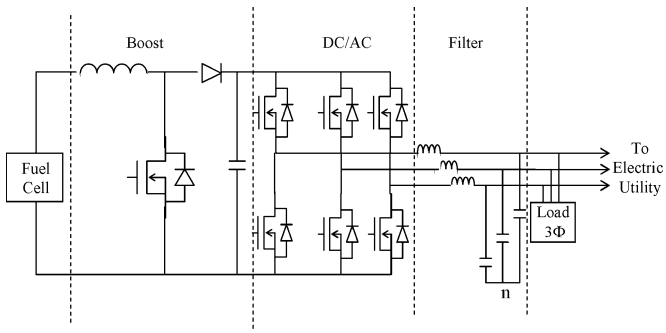

Fig. 4. Residential PES topology for the PSOFC PCS. The parameters of the power stage of the dc–dc boost converter and the VSI are listed in Table IV.

II. Overview of PSOFC-PCS Modeling and Interaction Analyses

To study the effects of load transients, a comprehensive model of the PSOFC-based PCS with the flow of data among various models, as shown in Fig. 3, is developed. The temporal models for the PSOFC, PES, which includes AL, and BOPS are implemented using an embedded MATLAB function, SimPowerSystems, and gPROMS[1], respectively.

The details of the transient models of SOFC, BOPS, PES, and AL are described in [4], [5], [7], [12].

The PES is responsible for processing the output voltage and current of the PSOFCS to a level that can be used by the AL. The PES topological model, as shown in Fig. 4, used for PSOFC-based PCS consists of a dc–dc boost converter to step up the PSOFCS output voltage followed by a dc–ac inverter.

The BOPS model[2], as shown in Fig. 5, consists of the FPS to convert natural gas to hydrogen (which is used as PSOFC fuel) and the thermal-management and power-recovery subsystems (TM/PRS) to maintain the fuel and the oxidant temperature for efficient chemical reactions in the PSOFCS. This model is used to analyze the thermodynamic, kinetic, geometric, and cost characteristics of the BOPS and its components at full- and part-loads. A representative schematic of the BOPS configuration is shown in Fig. 5. The actual configuration is a varied subset of

[1]gPROMS is a simulation software that incorporates several nonlinear solvers for dynamic process modeling and optimization. gPROMS is distributed by Process System Enterprises, Inc. (http://www.psenterprise.com/products_gproms.html).

[2]The BOPS model parameters and base-line conditions are extensive and are described in complete detail in [8], [12].

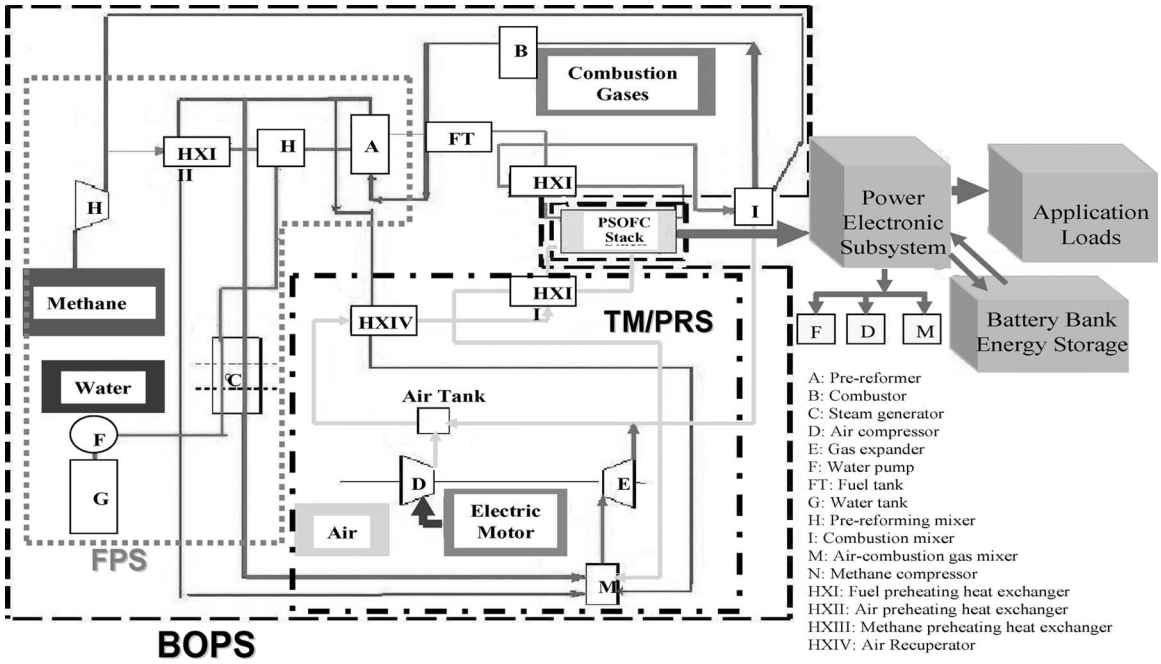

Fig. 5. Representative flow diagram of a methane-based BOPS model supplying fuel and air to the PSOFCS. The actual optimal BOPS configuration (a varied subset of the one shown in this figure) is not presented here due to pending patent considerations.

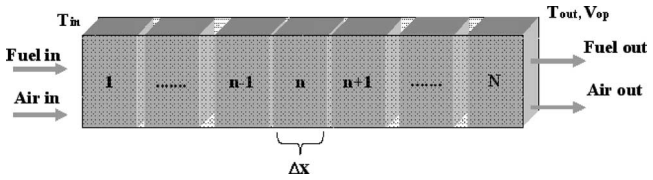

Fig. 6. 1-D homogenous slab model for the PSOFC providing 1-D discretizations involving finite differences. Temperature, current, and molar flow rates of air and fuel are calculated at each instance of time for $n = 1, \ldots, N$ [18]–[20].

this configuration and is not presented here due to pending patent considerations. The varied subset configuration is optimally determined based on the large-scale dynamic optimization of the synthesis/design and operational/control of the BOPS coupled to the fuel cell stack [15], [16].

To study the impact of load transients on the PSOFC, an accurate prediction of the parameters inside the cell is essential. As the transient model of the PSOFC [8] cannot predict the variation of different parameters inside the PSOFC, a spatio-temporal model of the PSOFC is developed, which provides one-dimensional (1-D) discretizations of a planar cell in Simulink using an embedded MATLAB function. The function is designed to accept the required system inputs (reactant stream flow rates, compositions, and temperatures, cell geometric parameters, and cell current) and return the corresponding properties of the output.

The fuel-stream and the air-stream inlet temperatures (as shown in Fig. 6) are used to calculate the temperature of the fuel cell structure at the inlet and to compute the temperature-dependent thermal conductivity and specific heat values. The bulk density of the stack has been used to account for the open channel volume fraction so that a thermal conduction model can be constructed as representative of a homogenous 1-D slab.

The PSOFC stack thermal transient is described by the "thermal energy equation"

$$\rho C_p \frac{\partial T}{\partial t} - k \frac{\partial^2 T}{\partial x^2} = Q \tag{1}$$

where Q represents the sum of the resistive heat rate per unit volume and the heat rate per unit volume generated by the electrochemical and shift reactions taking place within the cell, and ρ and C_p are the combined mass density and the combined specific heat capacity of the fluids and the solids (electrodes), respectively. Eq. (1) is solved along the length of the fuel cell as shown in Fig. 6, using a centered-difference approximation of the second derivative [17]

$$\frac{\partial^2 T}{\partial x^2} \approx \frac{1}{\Delta x^2}[T_{n+1,t} - 2T_{n,t} + T_{n-1,t}]. \tag{2}$$

Approximating the term $\partial T/\partial t$ as the temperature difference across a single time step and substituting (2) into (1) yields

$$T_{n,t+1} = T_{n,t} + \frac{k\Delta t}{\rho C_p \Delta x^2}(T_{n+1,t} - 2T_{n,t} + T_{n-1,t}) + \frac{\Delta t}{\rho C_p} Q. \tag{3}$$

Given the temperature distribution along the fuel cell at $t = 0$, (3) is used to advance the solution in time for each successive time step. These temperature solutions are then used to solve for the other variables that are not described by a partial differential equation. Boundary conditions are set such that the temperature at the inlet of the cell is equal to the inlet streams temperature, and at the outlet, the cell is radiating to an environment with a known ambient temperature. The stack enclosure temperature is set to 5 °C less than the inlet temperature ($T_\infty = T_{\text{in}} - 5$).

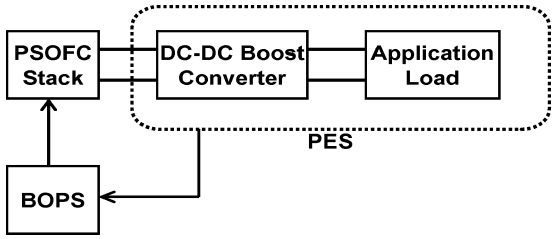

Fig. 7. PSOFCS connected to the load via a dc–dc boost converter.

Based on the temperature profile obtained using (3), the Nernst or reversible potential, cell resistance (using an Arrhenius fit of experimental data), current density, heat generation, updated flow rates, and reequilibration of the shift reaction are calculated at each of the nodal points representing a streamwise position in the PSOFC [18]–[20]. An operating voltage is assumed in order to compute the current density at each of the n discretized points in the cell, i.e.,

$$ji_n = \frac{(\mathrm{En}_n - V_n^{\mathrm{op}})}{\mathrm{ASR}_n} \tag{4}$$

where En is the Nernst potential, ASR represents the area-specific resistance (which is a temperature-dependent function), and V_{op} is the assumed output voltage. The Nernst potential is computed using the local temperature and composition-dependent values of the Gibb's free energy (ΔG) and is given by

$$\mathrm{En} = \frac{\Delta G}{mF} \tag{5}$$

where m is the stoichiometric coefficient of electrons in the electrochemical reaction and F is the Faraday's electrochemical constant. Using (4), the total cell current I is obtained by summing over all the computational unit cells as

$$I = \sum_{n=1}^{N} A_n ji_n. \tag{6}$$

Hydrogen utilization is directly proportional to the current and can be defined as

$$U = \frac{I}{\eta(mF)} \tag{7}$$

where η is the hydrogen molar flow rate, which is determined by the BOPS.

In order to compute an operating voltage V_{op} from the required PSOFC current, an iterative secant-root-finding method is employed, which varies the assumed operating voltage until the computed total current result matches the specified input current. The volumetric heat generation term Q in the heat equation is a combination of the ohmic heating due to current flow and the electrochemical heat of reaction, namely

$$Q = (V_{\mathrm{tn}} - V_{\mathrm{op}})ji \tag{8}$$

where the enthalpy of reaction (ΔH) is used to define the thermal neutral voltage (V_{tn})

$$V_{\mathrm{tn}} = \frac{\Delta H}{mF}. \tag{9}$$

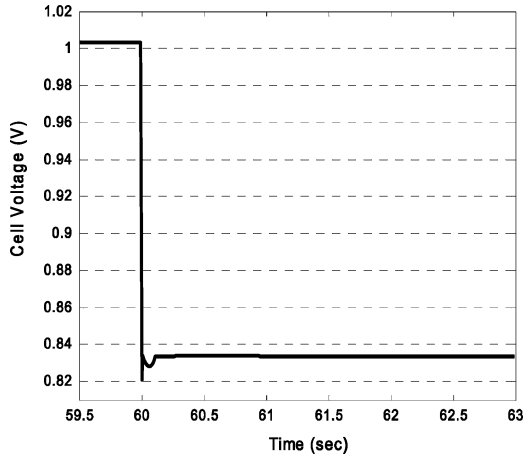

Fig. 8. Load/current transient (no-load to full-load current) that results in a drop in the PSOFC output voltage.

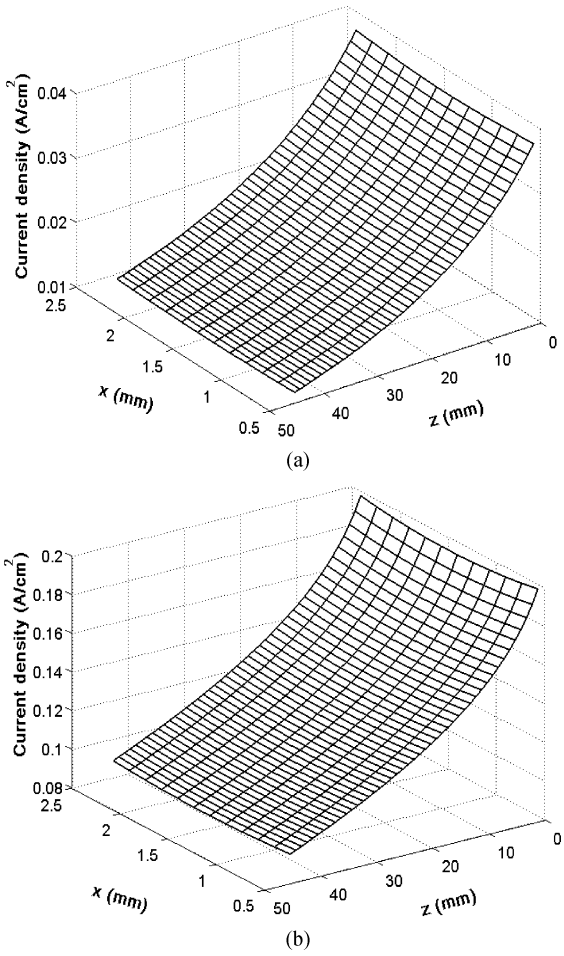

Fig. 9. Spatial current-density variation across the PSOFC cross section (a) Before. (b) After the load transient.

Air and fuel concentrations and flow rates entering a computational unit cell are taken to be the exit rate and composition of the upstream cell. It is assumed that the reactant streams and surrounding solids have a uniform temperature within each computational unit cell. A material balance within the cell accounts for the inlet and exit flows, along with the effect of the

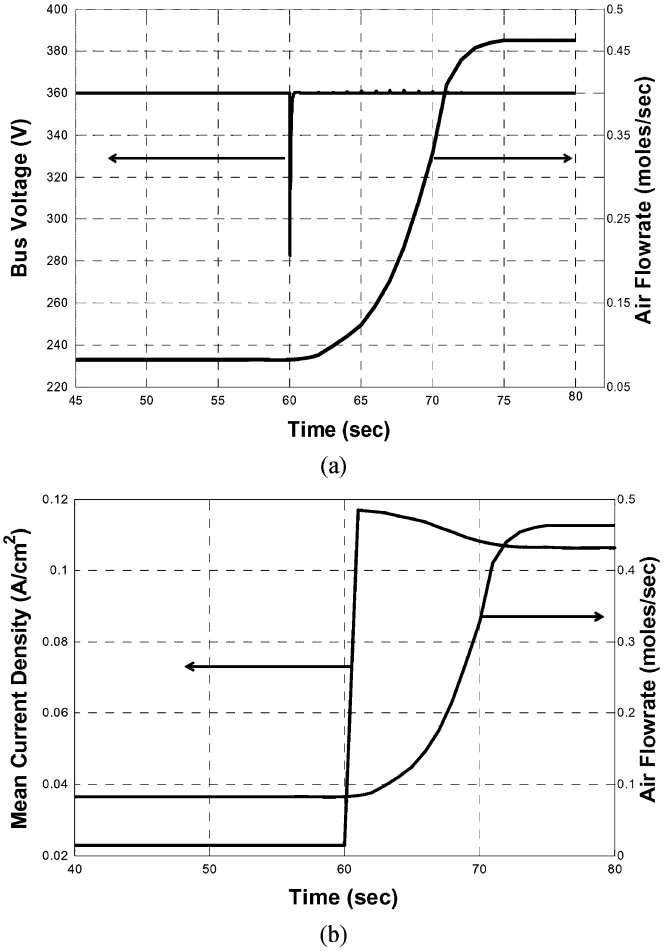

Fig. 10. Illustration of comparison of response times. (a) PES versus the BOPS. (b) PSOFC versus the BOPS.

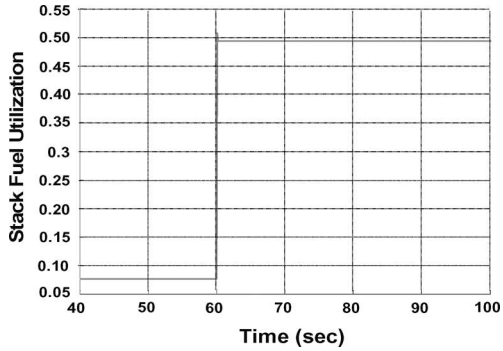

Fig. 11. Transient in the fuel (hydrogen) utilization due to the load transient.

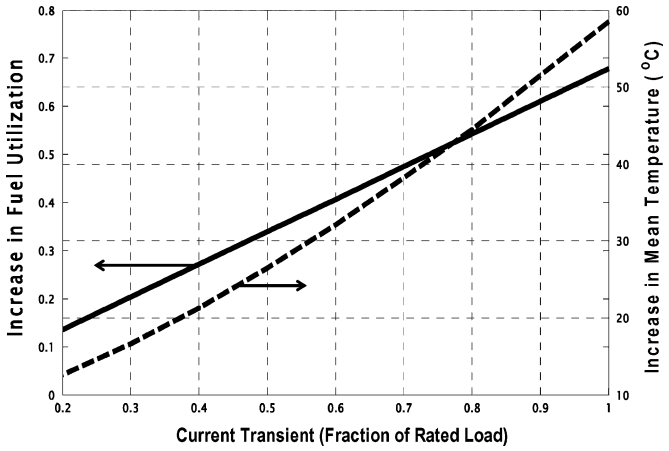

Fig. 12. Effect of severity of the load transient on the fuel (hydrogen) utilization and mean stack temperature.

electrochemical reaction and the equilibration of the water–gas shift reaction. The fuel value of CO is extracted by assuming that the water–gas shift reaction $(\mathrm{CO} + \mathrm{H_2O} \Leftrightarrow \mathrm{CO_2} + \mathrm{H_2})$, which proceeds rapidly under PSOFC operating conditions, remains in equilibrium. With the shift reaction in equilibrium, the Nernst potential calculated for CO oxidation will be equal to that calculated for hydrogen oxidation, so there would be no difference in the thermodynamic driving force for CO or H_2 electrochemical reactions, except for the kinetic differences.

The overall interaction analysis to ascertain the efficacy of energy-buffering devices and control techniques on the performance of PSOFC during a load transient is carried out in two steps. First, a time-domain analysis of the PSOFC-based PCS is carried out using the comprehensive model discussed and described in detail in [8], [12]. Using such a temporal analysis, the change in the PSOFCS output current and voltages before, during, and after a load transient is obtained.

To translate system-level electrical parameters of the PSOFCS to its cell-level electrochemical parameters [such as current density as in (4), fuel utilization as in (7), and cell temperature distributions as in (3)], a detailed finite element analysis (FEA) using the spatial model of the PSOFC is conducted. Because PSOFC parameters such as hydrogen depletion and cell temperature can directly affect the material properties of the PSOFC, it is important to study the spatial distribution of these parameters across its cross section.

III. SOFC Performance Analyses During Load Transient

A. Case I: Operation Without Battery Buffering

Fig. 7 shows the operating configuration for Case I. The PSOFC stack is connected to the dc–dc converter that feeds the load. For this investigation, the inverter (dc–ac converter) is removed. The scaled PSOFC PCS does not have any energy buffering as well. As such, the initial effect of a load transient directly affects the performance of the PSOFCS. This is analyzed using the models outlined in Section II.

Fig. 8 shows the drop in the output voltage of the PSOFC due to the load transient (40% of rated load current transient). The voltage drop is attributed to the enhanced polarization losses owing to higher current density, as illustrated in Fig. 9. Because the response time of the BOPS is significantly slower as compared to the response time of the PES/SOFC [21] [as illustrated in Fig. 10(a) and (b)], the input fuel flow rates of the PSOFCS will not change immediately after the load transient. This will lead to higher fuel utilization in the stack so as to attain a new electrochemical steady state.

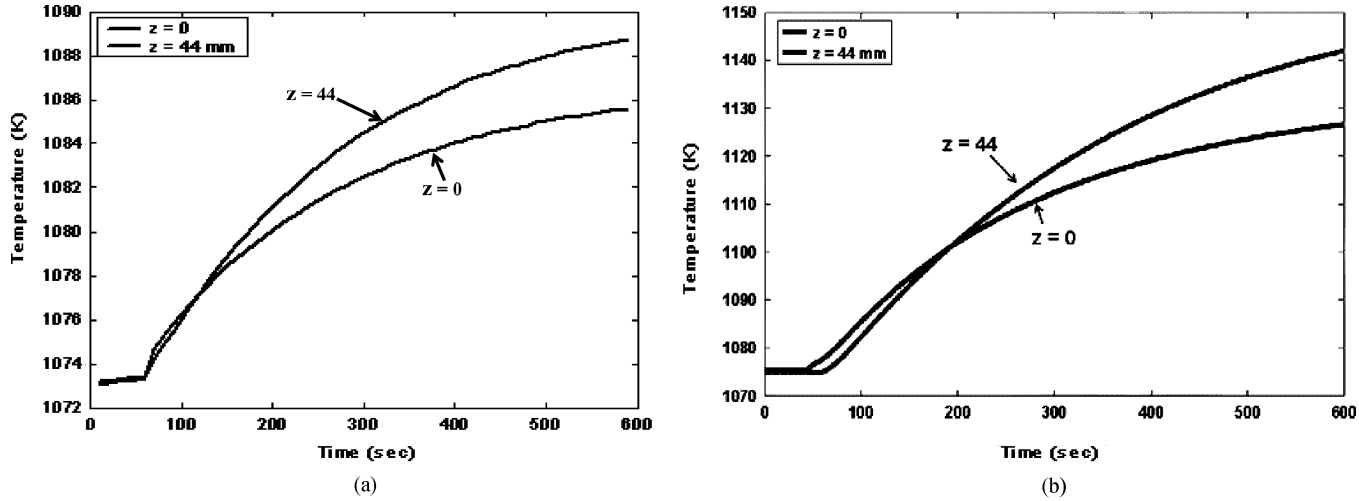

Fig. 13. Mean variation of temperature at the extreme ends of the PSOFC due to (a) 40% and (b) 100% of rated load current transient.

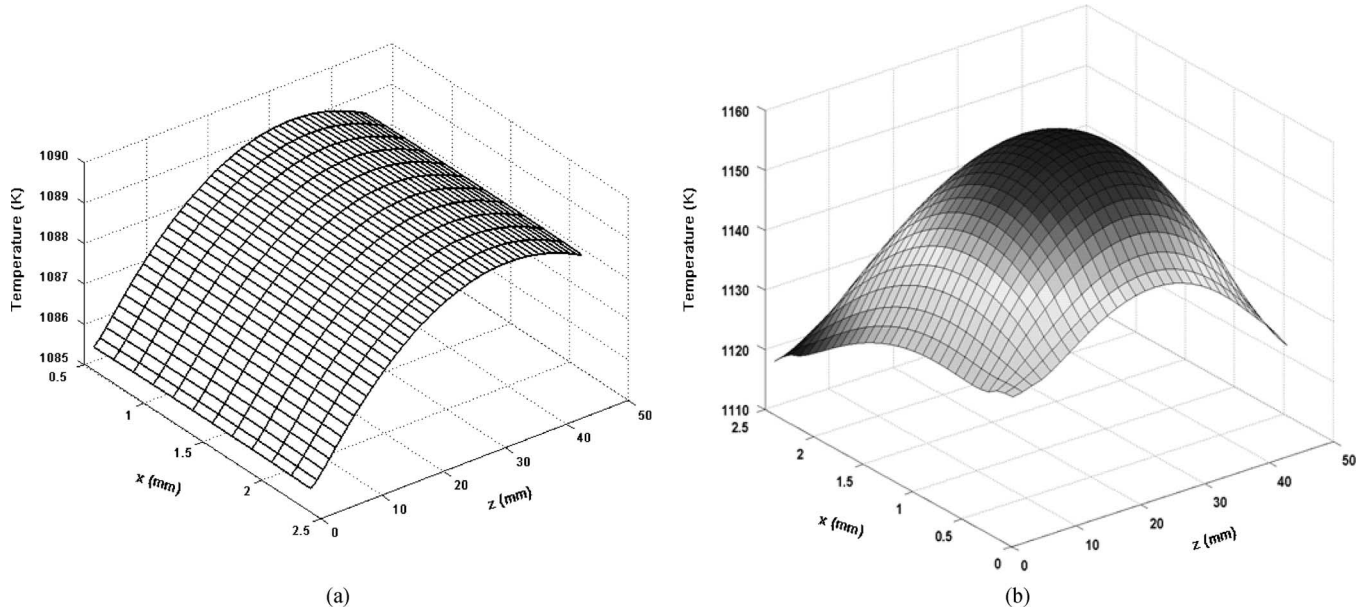

Fig. 14. Spatial temperature distribution across the PSOFC at time $t = 600$ s after (a) 40% and (b) 100% of rated load current transient.

TABLE I
RESIDUAL STRESSES AT PSOFC INTERFACES DUE TO RATED LOAD TRANSIENT

Interfaces	Maximum Tensile Stress (MPa)	
	Before Transient	After Transient
Anode interface with electrolyte	22.332	26.162
Electrolyte interface with anode	0.16	1.197
Electrolyte interface with cathode	14.563	57.413
Cathode interface with electrolyte	0.08	0.29

Fig. 11 shows that hydrogen utilization increases very sharply immediately after the load transient. The increase in the stack fuel utilization due to the load transient is dependent on the severity of the current transient, as shown in Fig. 12. To prevent the zero-reactant condition in the stack, the operating base fuel utilization of the stack needs to be lowered and this decreases the efficiency of the stack significantly.

The thermal energy balance at each node can be obtained using (3) with the assumption of a negligible temperature difference across the nodes, i.e.

$$T_{n,t+1} = T_{n,t} + \frac{\Delta t}{\rho C_p} Q \tag{10}$$

which shows that for a given value of ρ and C_p, an increase in Q[3] (because of the increased rate of exothermic reactions), until the BOPS responds to the increased demand of fuel and air, results in a rise in the fuel cell temperature. However, the thermal time constant of the PSOFC being much larger than that

[3]The variable Q, which is the net rate of energy transfer due to heat interactions and generation, increases with an increase in hydrogen utilization.

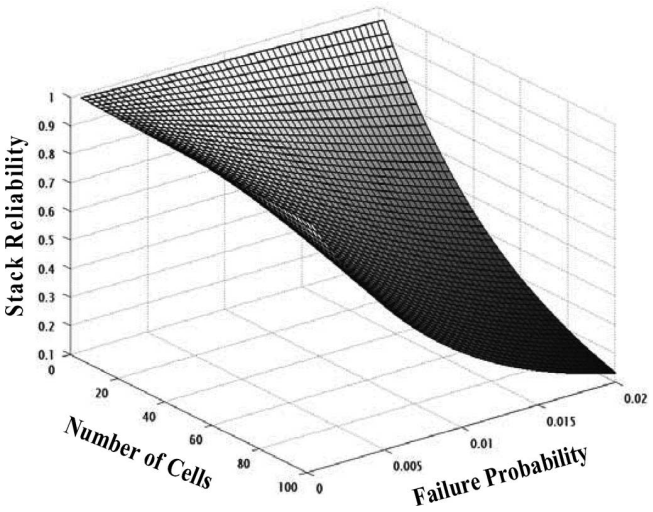

Fig. 15. Estimated stack reliability with probability of failure of a cell.

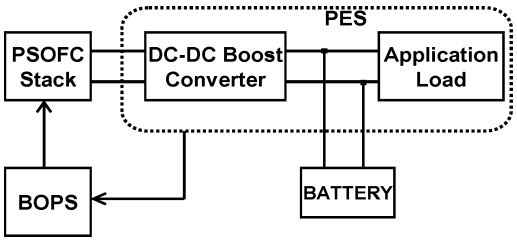

Fig. 16. PSOFCS connected to the load via a dc–dc boost converter. The battery provides the energy buffering during and after the load transient.

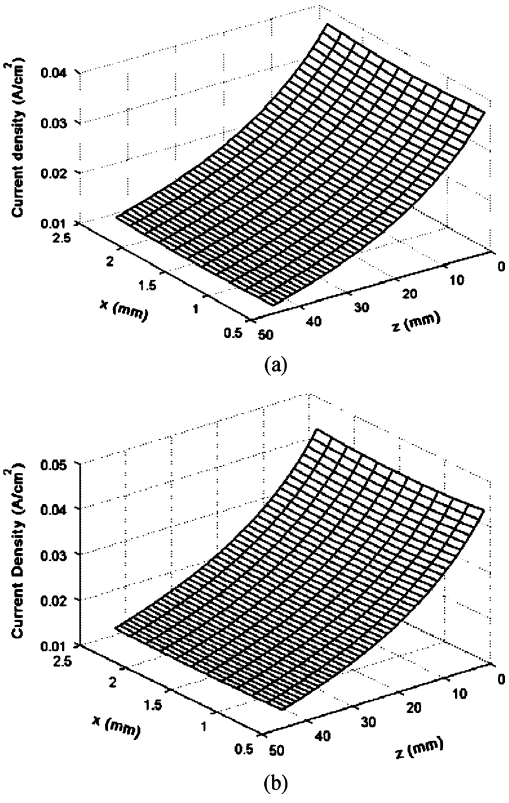

Fig. 17. Spatial distribution of current density across the cross section of the PSOFC (a) before and (b) after the load transient with battery buffering.

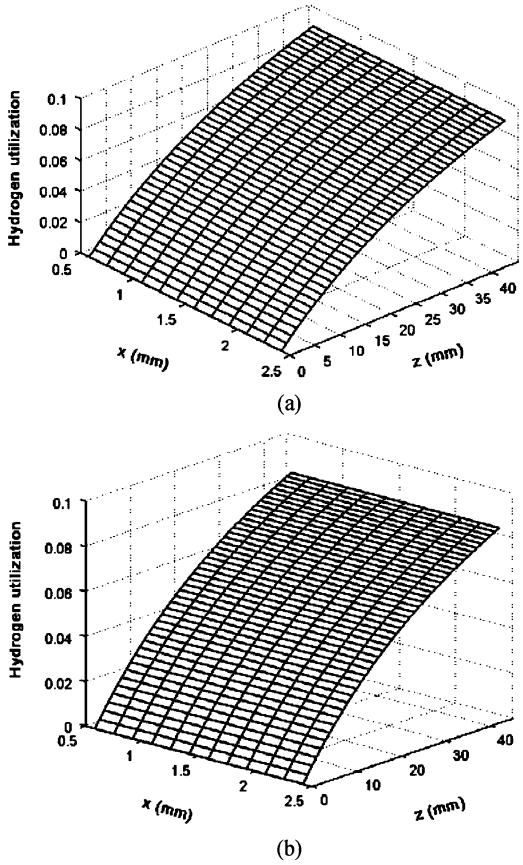

Fig. 18. Hydrogen utilization across the PSOFC (a) before and (b) after the load transient with battery buffering.

of the PSOFC electrochemical or PES time constants [20], the cell temperature will gradually increase, as validated in Fig. 13, until the PSOFC attains a new thermal steady state.

Fig. 14 shows the nonuniform spatial temperature distribution within the PSOFC after the load transients. The degree of nonuniformity in the temperature increases with the severity of the load transient, as shown in Fig. 14(b). A nonuniform increase in the cell temperature leads to a nonuniform expansion of the cell components due to the difference in their CTEs. In a PSOFC, with strict binding among each cell components, a slight mismatch in thermal expansion among the cell components can cause severe residual stress, which may degrade the performance and reliability of the cell [11].

A preliminary thermal analysis of the rated load transient reveals that significant residual tensile stress is developed at the interface of the electrolyte with the cathode, as given in Table I, leading to a cell failure probability of approximately 1%. The reliability of a PSOFCS depends on the reliability of the individual cells and the number of cells in the stack, and a slightest decrease in the reliability of the cells leads to a severe degradation in the stack reliability [22], as shown in Fig. 15.

The frequency of the load transient increases the severity of this effect on the life of the stack in the long run. Therefore, mitigation techniques are essential to alleviate these degrading effects of load transients on PSOFC.

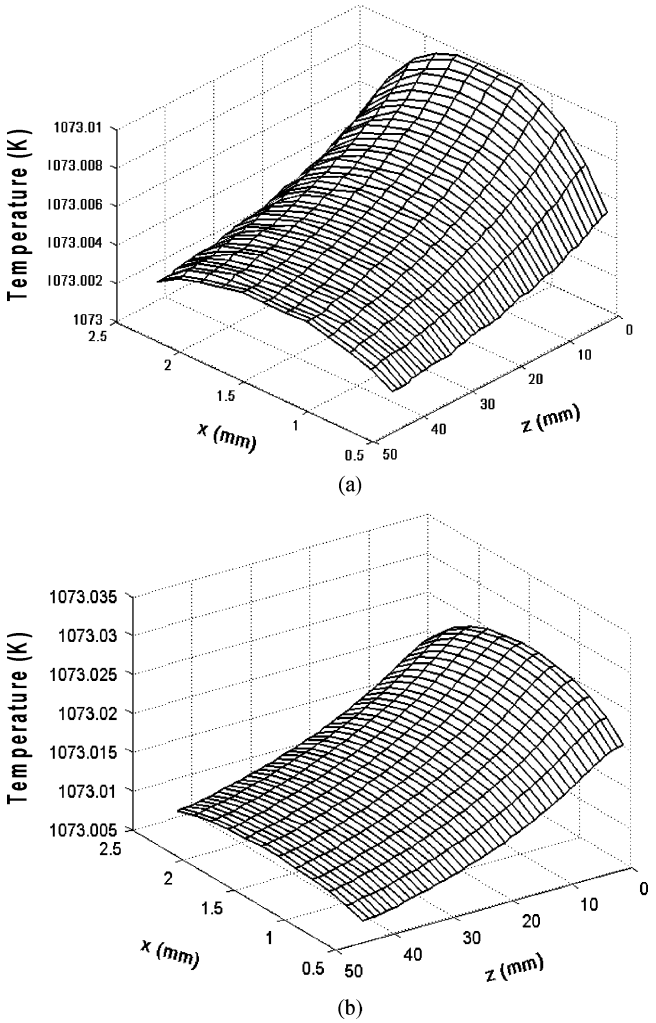

Fig. 19. Effect of battery buffering on the spatial variation of the temperature of the PSOFC (a) before and (b) after the load transient.

B. Case II: Operation With Battery Buffering

As the batteries (depending on their size) discharge at rapid rates, their operating life is small. However, fuel buffering using pressurized hydrogen (or reformate) tanks (PHTs) mitigates the effects of load transients by supplying fuel at the required rates to the PSOFCS for any load condition. Suitable reserves guarantee that the fuel in the tank is never depleted during and shortly after the transients until a new steady state is achieved. However, the size of a PHT is typically larger than that of a battery (although the weight may not be) and hence, it may be a less viable candidate for energy buffering depending on system-level volume constraints.[4]

Fig. 16 shows an arrangement to investigate the impact of a battery on the PSOFC during and after the load transient.

During a load transient, the battery supplies the additional energy requirements to the load till the BOPS responds, and hence, the load demands of the PSOFC are substantially reduced. Fig. 17 shows the current density of the PSOFC before and after the load transient. Clearly, unlike Fig. 9, the battery buffering ensures practically no change in the current density of the PSOFC after the transient. Consequently, the increase in fuel utilization as well as the accompanying nonuniformity in the spatial temperature distribution is negligible (as illustrated in Figs. 18 and 19) as opposed to the Case I results shown in Figs. 11 and 14. This eliminates the degrading effect of the low-reactant condition. Again, with such a small increase in the fuel utilization, the operating fuel utilization can be increased significantly to increase the efficiency of the stack. Thus, a battery provides the additional energy requirement of the load during a load transient, mitigating its degrading effects on the reliability and performance of PSOFC.

[4]In fact, a combination of both types of energy buffering which provides the optimal system solution should be obtained. It will depend, of course, on the trade-offs considered and the constraints that must be met.

TABLE II
BASELINE CONDITIONS FOR THE PSOFC MODEL

Pressure (atm)	3
Stoichiometric number	3
Open circuit voltage (V)	1.05
Inlet hydrogen mole fraction	0.45
Inlet carbon-monoxide mole fraction	0.12
Inlet steam mole fraction	0.11

TABLE III
INPUT OPERATING CONDITIONS OF THE PSOFC SPATIAL MODEL

Co/counterflow	
Hydrogen flow rate	1.2×10^{-6} mole/sec
Water flow rate	1.333×10^{-7} mole/sec
Oxygen flow rate	1.04×10^{-5} mole/sec
Nitrogen flow rate	4.2×10^{-5} mole/sec
Cell area	4.5 cm x 0.2 cm
Fuel/air inlet temperature	800 °C

IV. SUMMARY AND CONCLUSION

This paper investigates the effects of battery buffering on the reliability and performance of a PSOFC during load transients. It is observed that the post-load-transient cell current density increases significantly, which in turn results in a surge in the fuel utilization, leading to a nonuniform temperature increase in the PSOFC. The nonuniform temperature distribution induces potentially degrading residual stresses at the interfaces of the cell. An energy-buffering device (such as a battery) provides the excess energy required instantaneously, decreasing the load demands on the PSOFC stack, and in turn decreasing the fuel utilization level during the transients. The size of the battery should be optimally chosen so as to handle additional load current during the load transient and hence, to maintain the fuel utilization within certain limits till the BOPS responds. This ensures that the detrimental impacts on the materials of the PSOFC are avoided, resulting in improved reliability. Such a PSOFC-based PCS ensures better load following and hence, may lead to improved system performance and efficiency.

APPENDIX

See Tables II–IV.

TABLE IV
POWER-STAGE PARAMETERS FOR THE PES TOPOLOGY IN FIG. 4

Parameters	Values
DC-AC Converter	
Filter inductor	0.5 mH
Filter capacitor	0.5 mF
Switching frequency	10 kHz
DC-DC Converter	
Filter inductor	1 mH
Filter capacitor	1 mF
Switching frequency	10 kHz

REFERENCES

[1] *Fuel Cell Handbook,* 4th ed, Office of Fossil Energy, U.S. Department of Energy, 1998.

[2] J. A. Smith, M. H. Nehrir, V. Gerez, and S. R. Shaw, "A broad look at the workings, types, and applications of fuel cells," presented at the IEEE Power Eng. Soc. Summer Meet., Chicago, IL, 2002.

[3] S. C. Singhal and K. Kendall, *High Temperature Solid Oxide Fuel Cells: Fundamentals, Design and Applications*. New York: Elsevier, 2003.

[4] S. K. Mazumder, R. Burra, K. Acharya, M. R. von Spakovsky, D. J. Nelson, D. Rancruel, C. Haynes, and R. Williams, "Development of a comprehensive simulation platform to investigate system interactions among solid-oxide fuel cell, power-conditioning systems, and application loads," in *Proc. ASME 1st Int. Conf. Fuel Cell Sci. Eng. Technol.*, 2003, pp. 101–110.

[5] K. Acharya, S. K. Mazumder, R. Burra, R. Williams, and C. Haynes, "System-interaction analyses of solid-oxide fuel cell (SOFC) power-conditioning system," in *Proc. IEEE IAS Conf.*, 2003, vol. 3, pp. 2026–2032.

[6] K. Acharya, S. K. Mazumder, and R. Burra, "Impact of power-electronics systems on the performance and durability of tubular solid-oxide fuel cell," in *Proc. IEEE Appl. Power Electron. Conf.*, 2004, vol. 3, pp. 1515–1520.

[7] M. R. von Spakovsky, D. Rancruel, D. Nelson, S. K. Mazumder, R. Burra, K. Acharya, C. Haynes, R. Williams, and R. S. Gemmen, "Investigation of system and component performance and interaction issues for solid-oxide fuel cell based auxiliary power units responding to changes in application load," in *Proc. IEEE Ind. Electron. Conf.*, 2003, vol. 2, pp. 1574–1579.

[8] S. K. Mazumder, K. Acharya, C. Haynes, R. Williams, M. R. von Spakovsky, D. J. Nelson, D. F. Rancruel, J. Hartvigsen, and R. S. Gemmen, "Solid-oxide-fuel-cell performance and durability: Resolution of the effects of power-conditioning systems and application loads," *IEEE Trans. Power Electron.*, vol. 19, no. 5, pp. 1263–1278, 2004.

[9] E. A. Achenbach, "Response of a solid oxide fuel cell to load change," *J. Power Sources*, vol. 57, pp. 105–109, 1995.

[10] Y. C. Hsiao and J. R. Selman, "The degradation of SOFC electrodes," in *Proc. Solid State Ionics*, 1997, vol. 98, pp. 33–38.

[11] H. Yakabe, T. Ogiwara, M. Hishinuma, and I. Yasuda, "3D model calculation for planar SOFC," *J. Power Sources*, vol. 102, pp. 144–154, 2001.

[12] S. K. Mazumder, M. R. von Spakovsky, C. Haynes, K. Acharya, R. Burra, D. Rancruel, R. Williams, and D. Nelson, "An investigation to resolve the interaction between fuel cell, power conditioning system and application loads," Phase-I Topical Report, U.S. DoE, Cooperative Agreement Number: DE-FC26-02NT41574, Oct. 2003.

[13] S. H. Pyke, P. J. Howard, and R. T. Leah, "Planar SOFC technology: Stack design and development for lower cost and manufacturability," ALSTOM Research and Technology Centre, ETSU F/01/00194/REP, DTI/Pub URN 02/1350, 2002.

[14] L. J. Frost, R. M. Privette, and A. C. Khandkar, "Progress in the planar CPn SOFC system design," *J. Power Sources*, vol. 61, pp. 135–139, 1996.

[15] D. F. Rancruel and M. R. von Spakovsky, "Development and application of a dynamic decomposition strategy for the optimal synthesis/design and operational/control of a SOFC based APU under transient conditions," in *Proc. IMECE*, NY, Paper No. IMECE2005-82986, Nov. 2005, submitted for publication.

[16] D. F. Rancruel, "Dynamic synthesis/design and operation/control optimization approach applied to a solid oxide fuel cell based auxiliary power unit under transient conditions" Ph.D. dissertation, Virginia Polytechnic Inst. State Univ., VA, Feb. 2005.

[17] A. Constantinides and N. Mostoufi, *Numerical Methods for Chemical Engineers with Matlab Applications*. Englewood Cliffs, NJ: Prentice-Hall, 1999.

[18] J. Hartvigsen, S. Elangovan, and A. Khandkar, in *Science and Technology of Zirconia V*, S. Badwal, M. Bannister, and R. Hannink, Eds. Lancaster, PA: Technomic Publishing Company, 1993.

[19] I. V. Yentekakis, S. Neophytides, S. Seimanides, and C. G. Vayenas, "Mathematical modeling of cross-flow, counter-flow and cocurrent-flow solid oxide fuel cells: Theory and some preliminary experiments," in *Proc. 2nd Int. Symp. Solid Oxide Fuel Cells*, Athens, Greece, 1991, pp. 281–288.

[20] J. R. Ferguson in *Proc. 2nd Int. Symp. SOFCs*, 1991, p. 305.

[21] E. A. Liese, R. S. Gemmen, F. Jabbari, and J. Brouwer, "Technical development issues and dynamic modeling of gas turbine and fuel cell hybrid systems," in *Proc. Int. Gas Turbines Inst.*, 1999, 99-GT-360

[22] D. Stolten, "Comparison of SOFC and high temperature electrolysis," presented at the High Temp. Electrolysis IEA Meeting, San Antonio, Nov. 1–5, 2004.

Sudip K. Mazumder is currently the Director of Laboratory for Energy and Switching Electronics Systems and an Associate Professor in the Department of Electrical and Computer Engineering, University of Illinois, Chicago (UIC). He has over ten years of professional experience and has held Research and Development and Design positions in leading industrial organizations. His current research interests include interactive power electronics/power networks, renewable and alternate energy systems, and new device and systems-on-chip enabled higher power density.

Prof. Mazumder is an Associate Editor of the IEEE TRANSACTIONS ON INDUSTRIAL ELECTRONICS. He received the Department of Energy Solid State Energy Conversion Alliance Award, the National Science Foundation Career Award, and the Office of Naval Research (ONR) Young Investigator Award, in 2002, 2003, and 2005, respectively. He was also the recipient of the Prize Paper Award from the IEEE TRANSACTIONS ON POWER ELECTRONICS and the IEEE Power Electronics Society, in 2002. He has been invited for plenary and keynote lectures for several conferences.

Sanjaya K. Pradhan received the B.Tech. (Hons.) degree in energy engineering from the Indian Institute of Technology, Kharagpur, India.

He is currently pursuing the Ph.D. degree in electrical engineering at University of Illinois, Chicago. His research interests include interaction analysis of fuel cells power system, power system modeling, and control design for distributed energy system. He has two years of industry experience in the development of system software.

Joseph Hartvigsen received the M.S. degree in chemical engineering from Iowa State University, Ames.

He is the Senior Engineer in the solid-oxide fuel cells and Hydrogen Technologies group at Ceramatec, Inc. in Salt Lake City, UT. He has over 20 years of professional experience. He is currently Principal Investigator of a number of research projects relating to SOFC, fuel processing, and hydrogen production at Ceramatec. He has actively researched and published in the area of SOFC modeling since 1991. He is also active in the area of renewable energy. He previously worked in the defense aerospace industry at Boeing Military Airplanes, and Hercules Aerospace, performing analysis of solid rocket motors, hypersonic and stealth aircraft. He holds more than 12 patents and has published over 25 journals and conference papers.

Michael von Spakovsky is currently a Professor of Mechanical Engineering and Director of the Center for Energy Systems Research, Virginia Polytechnic Institute and State University, Blacksburg.

He has 17 years of teaching/research/industry experience. He is the author or coauthor of over 150 papers published in international journals. He has been invited for numerous talks worldwide.

Dr. von Spakovsky's is a Member of the American Institute of Aeronautics and Astronautics, a Fellow of the American Society of Mechanical Engineers (ASME), and an Elected Member of the SigmaXi and Tau Beta Pi. He has served as the Editor-in-Chief of the *International Journal of Thermodynamics*, and an Associate Editor of the *ASME Journal of Fuel Cell Science and Technology*.

Diego Rancruel received the M.S. and the Ph.D. degrees from Virginia Tech, Blacksburg, both in mechanical engineering. He has also a graduate degree in management.

He is currently a Technical Leader with General Electric Power Generation, Greenville, SC. He has eight years of industry experience, and has been involved in the development of energy systems, thermodynamic design, and aircraft systems optimization. His current research interests include developing transient analysis, creating operational philosophies, and generating new system concepts.